Atmos. Chem. Phys. Discuss., 12, 1019–1052, 2012
www.atmos-chem-phys-discuss.net/12/1019/2012/
doi:10.5194/acpd-12-1019-2012

Atmospheric Chemistry and Physics Discussions

Absorbing aerosols at high relative humidity: closure between hygroscopic growth and optical properties

J. M. Flores[1,2,*], **R. Z. Bar-Or**[3], **N. Bluvshtein**[3], **A. Abo-Riziq**[3], **A. Kostinski**[4], **S. Borrmann**[1,2], **I. Koren**[3], **and Y. Rudich**[3]

[1]Max Planck Institute for Chemistry, Particle Chemistry Department, Mainz, Germany
[2]University of Mainz, Institute for Atmospheric Physics, Mainz, Germany
[3]Weizmann Institute of Science, Dept. of Environmental Sciences, Rehovot, Israel
[4]Department of Physics, Michigan Technological University, Houghton, Michigan, USA
[*]now at: Weizmann Institute of Science, Dept. of Environmental Sciences, Rehovot, Israel

Received: 10 November 2011 – Accepted: 17 December 2011 – Published: 11 January 2012

Correspondence to: Y. Rudich (yinon.rudich@weizmann.ac.il)

Published by Copernicus Publications on behalf of the European Geosciences Union.

Abstract

The extinction coefficient and growth factor of humidified aerosols, at 80 % and 90 % RH, and at 532 nm and 355 nm wavelengths were measured for size-selected particles for ammonium sulfate, IHSS Pahokee peat (a lightly absorbing humic-like substance proxy), nigrosine (a black dye to model highly absorbing substances), and a mixture of AS and nigrosine. The ratio of the humidified extinction coefficients to the dry ($f\mathrm{RH}_{\mathrm{ext}}$(%RH, Dry)) was explored. The measured $f\mathrm{RH}_{\mathrm{ext}}$(%RH, Dry) was compared to theoretical calculations based on Mie theory, using the measured growth factors and assuming homogeneous mixing. The expected complex refractive indices (RIs) using the volume weighted mixing rule were compared to the RIs derived from the extinction measurements. Moreover, the differences between assuming a core-shell structure or a homogeneous mixing of the substances is examined. The laboratory results were used as a basis to model the change in the total extinction, the single scattering albedo (ω), and the asymmetry parameter (g) in the twilight zone of clouds at 355 nm and 532 nm.

We found slightly linear to no dependency of fRH(%RH, Dry) with size for absorbing substances in contrast to the decreasing exponential behavior with size for purely scattering substances. However, no discernable difference could be made between the two wavelengths used. Less than 5 % differences were found between the real parts of the complex refractive indices derived and those calculated using the volume weighted mixing rule, and the imaginary parts had up to a 20 % difference. Moreover, for substances with growth factor less than 1.15 there was, in average, less than 5 % difference between the extinction efficiencies calculated using a core-shell model and assuming homogeneous mixing for size parameters less than 2.5. For $x > 2.5$ the differences were greater causing and overestimation of the extinction efficiency (Q_{ext}) values if homogenous mixing was assume instead of a core-shell structure.

The total extinction as a function of distance from the nearest cloud was found to be independent from the imaginary component (k) of the dry RI of the absorbing aerosols

ACPD
12, 1019–1052, 2012

modeled. On the other hand, the single scattering albedo, as expected, decreased with larger values of k, whereas the asymmetry parameter increased suggesting a reduction in the reflectivity of the twilight zone with more absorbing aerosols and a reduction of cloud edge 3-D radiative effects.

1 Introduction

A major uncertainty in understanding Earth's climate system is the interaction between solar radiation and aerosols in the atmosphere. This interaction is dependent on the physical and chemical properties of the aerosols and the wavelength of the incident light. Furthermore, there is a complex interaction between clouds, aerosols and radiation that is still not well constrained. Koren et al. (2007) showed that a belt of forming and evaporating cloud fragments and hydrated aerosols extending kilometers away from the clouds into cloud-free areas could have major implications on how we calculate Earth's radiation budget. This phenomenon has been termed the "twilight zone". In the twilight zone, high relative humidity (RH) is predominant, creating an environment where aerosols can take up water and eventually deliquesce, grow and become more optically active. Also cloud droplets evaporate here leaving behind concentrated solution droplets and aerosol particles of complex chemical composition and of sizes with large optical effects. Moreover, the modeling of down welling solar irradiance at the surface relies on parameterizations of aerosol optical properties, mostly the single scattering albedo (ω) and the asymmetry parameter (g), and is a major source of discrepancy (Wild, 2005). Furthering our understanding of the optical properties of the hydrated aerosols can enable us to better model areas as the twilight zone as well as cloud-free areas with high RH.

Some laboratory studies have been devoted to understand the optical properties of purely scattering aerosols (mostly due to their "cooling effect") when exposed to high relative humidity. Garland et al. (2007) parameterized the relative humidity dependence of light extinction at 532 nm for inorganic ammonium sulfate aerosols; while Baynard

ACPD
12, 1019–1052, 2012

et al. (2006) looked at mixtures of NaCl and ammonium sulfate with a few dicarboxylic acids. Recently, Hasenkopf et al. (2011) compared the optical growth at 532 nm of slightly absorbing organic particles likely to have been present on early Earth and Titan.

Absorbing aerosols transform the solar electromagnetic energy to thermal energy, and therefore heating the aerosol layer while cooling (stabling) the atmosphere below it (Hansen et al., 2005). This can affect cloud formation (Koren et al., 2004); hence, it is crucial to better understand their optical properties and their RH dependence. While several studies have been directed to investigate the properties of absorbing aerosols such as organics (Kanakidou et al., 2005), dust (Kaufman et al., 2005; Yu et al., 2006), and soot (Jacobson, 2001; Koren et al., 2004; Menon et al., 2002; Jacobson, 2006), our level of understanding as the RH changes is still limited.

With the development of cavity ring down spectroscopy (CRDS), the extinction coefficient (extinction = scattering + absorption) of aerosols can be directly measured (Dinar et al., 2008; Lack et al., 2006; Lang-Yona et al., 2009; Pettersson et al., 2004; Riziq et al., 2007; Sappey et al., 1998; Smith and Atkinson, 2001). By measuring the total extinction of a substance at different sizes, and using Mie theory, the complex refractive index of the particles can be retrieved (Lack et al., 2006; Lang-Yona et al., 2009; Lang-Yona et al., 2010; Pettersson et al., 2004; Riziq et al., 2007). The complex refractive index (RI, $m = n + i\ k$) describes the scattering (real part, n) and absorption (imaginary part, k) of a substance. At different RH values, water uptake by atmospheric aerosols can occur; hence, changing their size and composition. This in turn will change the complex refractive index of the aerosols. To accurately predict the "new" complex RI different theoretical mixing rules are often used (Erlick, 2006). The most common rule being the volume weighted mixing rule. It is often used in chemical transport models that estimate the aerosol direct forcing (Haywood et al., 1997; Liu et al., 2007b), and in some laboratory studies. Riziq et al. (2007) measured different organic mixtures to test the validity of this mixing rule for a solution (before atomizing the particles). Garland et al. (2007) used the volume weighted mixing rule (assuming complete mixing of

ACPD
12, 1019–1052, 2012

the aerosols as they passed through a humidification stage) to test the performance of their system and to parameterize the change in the extinction coefficient when purely scattering substances (inorganic and organic) were exposed to an RH of 80 %.

In this work we perform a closure study between aerosol hygroscopicity and optical properties. We explore the validity of the mixing rules for water soluble absorbing aerosols, and address the change in refractive index of absorbing aerosols when exposed to 80 % and 90 % relative humidities, at 355 nm and 532 nm wavelengths. By doing so, we attempt at reaching closure between measured hygroscopic growth (by tandem hygroscopic DMA measurements), measured extinction (by CRD) and model calculations in order to study the ability to predict the optical properties of hydrated aerosols with different absorption extent. Moreover, we investigate how does the ratio of the extinction coefficient of the humidified aerosols to the dry extinction coefficient change as a function of size. We also test a core-shell structure model to explore the differences between the models for substances with low growth factors, under these hydration conditions. Finally, we apply the models to investigate how the twilight zone of warm clouds would change if aerosols with different degrees of absorption, from purely scattering to highly absorbing, at given hygroscopicity parameters κ (Peters and Kreidenweis, 2007), are present.

2 Methodology

To study the RH dependence of aerosols' optical extinction at 532 nm and 355 nm, a cavity ring down (CRD), and a scanning mobility particle sizer (SMPS; TSI model 3081) were used. A schematic of the laboratory setup is shown in Fig. 1. A full description of the CRD used in this study can be found in Riziq et al. (2007). Briefly, two plano-concave highly reflective mirrors (Los Gatos) are mounted at both ends of a stainless steel tube. The third harmonic (355 nm) or the second harmonic (532 nm) of an Nd:YAG (10 Hz, 3–6 ns, Ekspla) are introduced into the cavity though one end, the pulse of light in the cavity bounces back and forth, and by placing a photomultiplier at other

ACPD
12, 1019–1052, 2012

end of the cavity, the intensity of the light exiting the cavity is measured. The time it takes the initial intensity of the light to decay $1/e$ is then measured. By measuring the empty cavity (filled only with the carrier gas) decay time (τ_o) and the decay time filled with aerosols (τ) the extinction coefficient can be directly measured (Pettersson et al., 2004;Riziq et al., 2007):

$$\alpha_{\text{ext}} = \frac{L}{c\text{d}}\left[\frac{1}{\tau} - \frac{1}{\tau_0}\right] \quad (1)$$

where L is the length of the cavity, d is the distance filled with aerosols, and c is the speed of light.

Quasi-monodisperse particle distributions were generated by atomizing aqueous solutions of the compounds of interest with a TSI constant output atomizer (TSI-3076, 35 psi, 2.5 standard liters per minute (SLM) flow), the aerosol population is subsequently dried (RH < 3 %), passed through a neutralizer (TSI 3012A) to obtain an equilibrium charge distribution on the particles, and size selected with a differential mobility particle sizer (DMA, TSI model 3081). The dry, size selected aerosols exiting the DMA were diluted and directed to a deliquescence stage consisting of a saturated permeable membrane at a controlled temperature before being sampled by the CRD-SMPS system. Aerosol losses were measured with different sizes of polystyrene latex spheres (from 200 nm up to 800 nm) by placing a condensation particle counter (CPC; TSI Model 3022) before the CRD, and comparing the particle number concentration of this CPC with another CPC located at the end of the system; differences in particle concentration of less than 2 % were found. To avoid temperature fluctuations in the system, insulation was placed around the tubing, the CRD, and SMPS (represented by the shaded areas in Fig. 1). The relative humidity and temperature were measured at the exit of the humidification stage, within the CRD, and at the entrance of the sheath flow of the DMA in the SMPS system. Measurements were only taken when all measured RH values in the system were within 2 % (RH meter manufacture uncertainties are ±3 %RH for $10 \leq$ %RH ≤ 90). Following the deliquescence stage the

ACPD
12, 1019–1052, 2012

aerosols' RH dependent extinction coefficient ($\alpha_{ext,\%RH}$) was measured with the CRD and the hygroscopic growth factor (GF) was measured with the SMPS. The aerosol number concentrations were also measured with a CPC at the outlet of the CRD.

The substances were measured at eight different mobility diameters, from 200 nm to 550 nm in 50 nm steps, and 2 different RH values; 80 % and 90 %. The sequence of measurements was performed by first measuring the different diameters of a substance in a dry state (RH < 3 %), then directing the sample flow through the humidifier, allowing the system to equilibrate at the desired RH, and repeating the measurement for the same diameters. After the hydrated experiments were done, the dry measurement was repeated to check the stability of the system. If the final dry measurement differed more than 5 % from the initial, the measurements of that substance were repeated. Particle concentrations were kept below 1000 p cm^{-3}, and the median diameter from the SMPS size distributions (D_{med}) was taken instead of the chosen mobility diameter from the first DMA in order to reduce biases arising from multiply-charged particles (Hoppel, 1978). For this, a solution concentration of 500 mg l^{-1} for sizes between 200 nm to 300 nm was used, and for larger diameters, 350 nm to 550 nm, a 1000 mg l^{-1} concentration solution was used.

The hygroscopic growth is represented by the relative increase in the mobility diameter of particles due to water up take at a specific %RH:

$$\mathrm{GF}(\%\ \mathrm{RH}, \mathrm{Dry}) = \frac{D_{\%\ \mathrm{RH}}(\mathrm{RH})}{D_{\mathrm{dry}}} \quad (2)$$

where $D_{\%RH}$(RH) is the mobility diameter at a specific %RH, and D_{dry} is the dry measured mobility diameter. The GF of a mixture (GF_{mix}) can be estimated from the GFs of the pure components and their respective volume fractions (ε) using the Zdanovskii-Stokes-Robinson relation (ZSR relation; Sjogren et al., 2007; Stokes, 1966):

$$\mathrm{GF}_{\mathrm{mix}} = \left(\sum_j \varepsilon_j \mathrm{GF}_j^3 \right)^{\frac{1}{3}} \quad (3)$$

ACPD
12, 1019–1052, 2012

where the subscript j represents the different substances. The model assumes spherical particles, ideal mixing (i.e. no volume change upon mixing) and independent water uptake of the organic and inorganic components.

The changes of the aerosols optical properties due to hygroscopic growth is represented by the ratio of the measured extinction coefficient (α_{ext}, Mm^{-1}) at a specific %RH to the dry measurement, expressed as:

$$f\mathrm{RH}_{ext}(\%\mathrm{RH}, \mathrm{Dry}) = \frac{\alpha_{ext}(\%\mathrm{RH})}{\alpha_{ext}\,(\mathrm{Dry})} \quad (4)$$

where α_{ext}(%RH) is the extinction coefficient at a specific RH, and α_{ext}(Dry) is the extinction coefficient measured at an RH < 3 %. The extinction coefficient for homogenous spheres is described by:

$$\alpha_{ext} = \frac{1}{4}\pi N D^2 Q_{ext} \quad (5)$$

where N is the particle concentration, D the particle's diameter, and Q_{ext} the extinction efficiency. Hence, inserting Eqs. (2) and (5) into (4), Eq. (4) can be written as:

$$f\mathrm{RH}_{ext}(\%\mathrm{RH}, \mathrm{Dry}) = \frac{N_{\%\mathrm{RH}} Q_{ext-\%\mathrm{RH}}}{N_{\mathrm{Dry}} Q_{ext-dry}} \mathrm{GF}^2 \quad (6)$$

Three different substances were use d to measure the optical extinction growth, $f\mathrm{RH}_{ext}$(%RH, Dry), dependence with size and degree of absorbance: ammonium sulfate (AS), a purely scattering substance, was used to check the system performance; nigrosine, an organic black dye used as a model for highly absorbing substances; and IHSS Pahokee Peat (Pahokee), a fulvic acid used as a model for humic-like substances, or complex organic matter often found in aerosol (Dinar et al., 2007). A mixture of ammonium sulfate and nigrosine 1:1 molar ratio (AS:Nig), was also measured to investigate the variation in the imaginary part of the complex refractive index.

ACPD
12, 1019–1052, 2012

3 System validation with ammonium sulfate

The measurements of $f\mathrm{RH}_{\mathrm{ext}}$(%RH, Dry) with the system described above were validated with ammonium sulfate at 80 % RH. Figure 2 compares the measured $f\mathrm{RH}_{\mathrm{ext}}$(80 %RH, Dry) in this study, to that reported by Garland et al. (2007) and to the calculated $f\mathrm{RH}_{\mathrm{ext}}$(80 %RH, Dry) based on the measured GFs from the SMPS.

To convert the GFs to $f\mathrm{RH}_{\mathrm{ext}}$(RH, dry), the same method as described in Garland et al. (2007) was applied. Briefly, by using Mie scattering calculations (Bohren and Huffman, 1983), the extinction cross section of the dry aerosol were calculated with the refractive indices (RIs) retrieved from the dry CRD measurements of AS. Humidity-controlled, tandem SMPS measurements were used to determine the hygroscopic GF of size-selected aerosols and consequently to determine the volume fraction of water; i.e., the volume fraction of AS is known from the diameter measured by the first SMPS for the dry aerosols, and the total volume of the humidified AS particle (water + AS) is known from the (second) humidified SMPS measurements. Applying the volume weighted mixing rule for refractive indices,

$$n_{\mathrm{mix}} = V^{\mathrm{frac}}_{\mathrm{Dry}} n_{\mathrm{Dry}} + V^{\mathrm{frac}}_{\mathrm{water}} n_{\mathrm{water}} = \frac{D^3_{\mathrm{dry}} n_{\mathrm{dry}} + (D^3_{\mathrm{wet}} - D^3_{\mathrm{dry}}) n_{\mathrm{water}}}{D^3_{\mathrm{wet}}} \quad \textbf{(7a)}$$

$$k_{\mathrm{mix}} = V^{\mathrm{frac}}_{\mathrm{Dry}} k_{\mathrm{Dry}} + V^{\mathrm{frac}}_{\mathrm{water}} k_{\mathrm{water}} = \frac{D^3_{\mathrm{dry}} k_{\mathrm{dry}} + (D^3_{\mathrm{wet}} - D^3_{\mathrm{dry}}) k_{\mathrm{water}}}{D^3_{\mathrm{wet}}} \quad \textbf{(7b)}$$

where V_i^{frac} is the volume fraction of each component, with the optical properties of pure AS and water as input, the refractive indices for the humidified aerosol at different RHs were calculated (see Table 1). Finally, the new RI and new diameters, $D_{\%\mathrm{RH}} = \mathrm{GF} \times D_{\mathrm{dry}}$, where D_{dry} is the diameter measured by the SMPS for the dry aerosols, are taken to determine the humidified extinction cross sections at a wavelength of 532 nm. The ratio of the humidified extinction cross section curve to the dry

ACPD
12, 1019–1052, 2012

AS curve gives the theoretical $f\mathrm{RH}_{\mathrm{ext}}$ (80 %RH, Dry). The refractive index used for AS and water at 532 nm were $m = 1.504 + i0.0$ (derived from the dry measurements) and RI of $m = 1.335 + i0.0$ (Daimon and Masumura, 2007), respectively. The reported uncertainties in the measured $f\mathrm{RH}_{\mathrm{ext}}$(RH, dry) were based on the uncertainty in the RH measurement (±3 % RH), the SMPS size distributions (∼ ±1 %), and the uncertainty in the measured extinction coefficient from the CRD (∼ ±2 %). The GFs from each diameter were averaged to obtain a range in the theoretical calculations of $f\mathrm{RH}_{\mathrm{ext}}$; this is represented by the shaded area in Fig. 2.

It can be seen in Fig. 2 that the measured $f\mathrm{RH}_{\mathrm{ext}}$(80 % RH, Dry) values (every measured value is an average of at least 2 min with an extinction measurement made every 10.1 seconds) are in very good agreement with the $f\mathrm{RH}_{\mathrm{ext}}$(80 % RH, Dry) measured by Garland et al. (2007), and with the theoretical calculations. There is a slight overestimation at 200 nm, which may be attributed to the presence of larger doubly charged aerosols in the initial size selection. The good agreement between the theoretical calculations and the measured values suggests the experimental setup is reliable.

4 Results

4.1 Optical growth of humidified absorbing aerosols

The size dependence of $f\mathrm{RH}_{\mathrm{ext}}$ at 80 % and 90 % RH was studied for substances with different degrees of absorption at 532 nm and 355 nm. The GF values were converted to theoretical $f\mathrm{RH}_{\mathrm{ext}}$(%RH, Dry) as described for the 532 nm AS measurement at 80 % RH. Figure 3 shows the size dependence of $f\mathrm{RH}_{\mathrm{ext}}$(80 %RH, Dry) and $f\mathrm{RH}_{\mathrm{ext}}$(90 %RH, Dry) for pure AS, IHSS Pahokee Peat, a mixture of AS and nigrosine at a 1:1 molar ratio, and pure nigrosine dye for 80 % (left) and 90 % (right) RH at 532 nm (green full markers and patterned shaded area) and 355 nm (blue open markers and full shaded area). The measured growth factors obtained with the SMPS for each substance are presented in the legend. The reported ranges for the converted values (shaded areas

ACPD
12, 1019–1052, 2012

in Fig. 3) are based on the values calculated from the lower and upper limits of the uncertainty of the measured GFs.

The measurements for all substances at both RHs and wavelengths are in good qualitative agreement with the calculations. While there are some values which are outside of the shaded area all substances follow the theoretical trends. The measurement for the Pahokee peat for 355 nm at 90 % RH could not be completed due to shortage of substance, the measurement presented was performed at an RH = 95 % (±3 %).

The ammonium sulfate measurements show an exponential behavior of $f\mathrm{RH}_{\mathrm{ext}}$(80 %RH, Dry) and $f\mathrm{RH}_{\mathrm{ext}}$(90 %RH, Dry) with size. Garland et al. (2007) parameterized AS at 80 % RH with an exponential function. This study shows that the exponential behavior is also maintained at 90 % RH for 355 nm and 532 nm, as can be seen in Fig. 3. Additionally, the $f\mathrm{RH}_{\mathrm{ext}}$(80 %RH, Dry) and $f\mathrm{RH}_{\mathrm{ext}}$(90 %RH, Dry) values at 532 nm are greater than at 355 nm. The spectral independence of AS on wavelength might incorrectly lead to expect the same $f\mathrm{RH}_{\mathrm{ext}}$(%RH, Dry) curve for both wavelengths, however, the differences are attributed to the shape of the Mie curves and to the fact that the size parameters ($x = \pi D/\lambda$) for the diameters measured are larger at $\lambda = 355$ nm than at $\lambda = 532$ nm. For purely scattering substances, the extinction efficiency increases rapidly for size parameters smaller than 3, and the slope of this increase is steeper as the real part of the RI is larger. At 355 nm, the initial dry diameters measured have a greater extinction efficiency than at 532 nm, making $f\mathrm{RH}_{\mathrm{ext}}$(%RH, Dry) smaller at 355 nm than at 532 nm.

4.2 Validation of the volume weighted optical mixing rule

Figure 3 shows, in general, good qualitative agreement between measurements and theoretical calculations using the measured GFs, assuming homogenous mixing, and using the volume weighted mixing rule to calculate the corresponding complex refractive indices. A quantitative analysis was done by comparing the RI values obtained from the measurements with various Mie models that assume different mixing states or structures. These calculations may serve as a further verification for the commonly

ACPD
12, 1019–1052, 2012

used assumption of homogenously mixed particles at high %RH values. To retrieve the RI from the CRD measurements, the extinction efficiency of the humidified aerosols ($Q_{ext-\%RH}$) was calculated from the measured GF and the extinction coefficient at every diameter. By knowing the value of Q_{ext} at different diameters for internally mixed aerosols, a refractive index can be retrieved (Lang-Yona et al., 2009; Pettersson et al., 2004; Riziq et al., 2007). Figure 4 shows two examples of the results of the complex RI derivation and comparison performed. Four sets of data of Q_{ext} versus size at 532 nm and 80 % RH for the IHSS Pahokee Peat and nigrosine aerosol are presented: (1) The measured $Q_{ext,80\%RH}$ values obtained by the CRD and the measured $D_{80\%RH}$, (2) the complex RI retrieved from the $Q_{ext,80\%RH}$ measurements, using the method described in Riziq et al. (2007), (3) the Q_{ext} curve for the complex RI calculated assuming homogeneous mixing and applying a volume weighted mixing rule, where the RI for the Pahokee peat and nigrosine aerosols were retrieved from the dry measurements, and the RI value used for water at 532 nm was $m = 1.335 + i0.0$ (Daimon and Masumura, 2007), and (4) the Q_{ext} values assuming a core-shell structure for each measured diameter. The same analysis was performed for the other substances at both RHs and wavelengths. The RI used for water at 355 nm was $m = 1.349 + i0.0$ (Daimon and Masumura, 2007). The results are summarized in Table 1, which also provides for comparison literature growth factor values (when available), ZSR relation calculations, and the percent difference among the different measurements. The data in the table is presented in increasing degree of absorption of the proxy aerosols, from AS (no absorption) to Pahokee Peat to AS:Ng 1:1 and to pure nigrosine (highly absorbing). The retrieved complex refractive indices for most substances at both RHs are in good agreement with the calculated complex RI from the volume weighted averages; the real part of the RIs are within 5.3 % of each other. There are greater differences in the imaginary parts, but the values are within measurement errors.

For the IHSS Pahokee peat and nigrosine aerosols, there is an overestimation of the imaginary part at both wavelengths and RHs. Both substances have a small GF, which raises the question of their internal structures after humidification. Is there a

ACPD
12, 1019–1052, 2012

complete mixture within these particles or a small shell of water formed around the particles forming a core-shell structure which is consequently being measured by the CRD? To explore whether there could be an optical distinction for Pahokee peat and nigrosine if we assume a core-shell structure or complete mixing, the extinction efficiency as a function of size parameter was calculated separately for each case. For the homogenously mixed case, $Q_{\text{ext-homogeneous}}$ was calculated with the RI obtained from the volume weighted mixing rule. For the core-shell structure, $Q_{\text{ext-core-shell}}$ was calculated using the diameter measured after humidification as the total diameter, and the diameter selected from the first DMA as the core diameter. The RI of the core was taken from the dry measurements, and the RI of water was used for the RI of the shell. The code by Liu et al. (2007a) and Bohren and Hoffmann (1983) were used to calculate $Q_{\text{ext-core-shell}}$ and $Q_{\text{ext-homogeneous}}$, respectively. The ratio of $Q_{\text{ext-core-shell}}$ to $Q_{\text{ext-homogeneous}}$ was calculated and plotted as a function of size parameter for both wavelengths in Fig. 5. At 80 % RH, where Pahokee and nigrosine only grew 9 % and 12 %, respectively, there is less than a 5 % difference between the values obtained with a core-shell structure and those obtained by assuming homogenous mixture for size parameters less than 2.5. For 90 % RH, the differences between the core-shell structure and a homogeneously mixed particle are more noticeable, with up to a 7 % difference for the Pahokee peat. A clear distinction between the two mixing states can be observed at size parameters greater than 3. Mie curves of homogenously mixed particles with similar real part of the RI will have the maximum Q_{ext} value around the same size parameters, for real parts between 1.65 and 1.55 (the real parts of the RIs of Pahokee peat and nigrosine are between these values) the Q_{ext} peaks start around a size parameter of 2.5. For example, for purely scattering substances the maximums will be a series of resonance peaks. As the imaginary part of the complex RI increases the Q_{ext} peaks will accordingly decrease. Hence, if a substance is assumed to be homogenously mixed, when its internal structure is in reality a core-shell, the measured Q_{ext} will be lower and it will result in an underestimation of the imaginary part of the complex refractive index when it is calculated with the volume weighted mixing rule.

ACPD
12, 1019–1052, 2012

This can be seen in Fig. 4b for nigrosine, where the difference between the measurements (open circles) and the homogeneous assumption (solid line) is greater at larger size parameters, and by having assumed a homogenous mixture the imaginary part of the RI was slightly underestimated.

However, for Pahokee peat a core-shell structure does not seem to explain adequately the results. From Fig. 4a and Table 1 we can observe that the imaginary part of the retrieved complex RI for Pahokee peat at 80 % RH and 532nm is higher than for the dry substance. With a GF of only 1.09 there is the possibility that only small water clusters formed instead of a complete layer of water around the aerosols. Unfortunately, with the experiments performed in this study there is not enough information to examine the hypothesis.

5 Absorbing aerosol in the twilight zone

The "twilight zone" of clouds (Koren et al., 2007) is the transition area between clouds and the cloud-free atmosphere, which is affected by forming and evaporating cloud fragments and hydrated aerosols, and cloud 3-D radiative effects (Marshak et al., 2006; Varnai and Marshak, 2009). It was suggested that the twilight zone can extend kilometers away from the clouds affecting optical retrievals up to 30 km from the nearest cloud edge (Koren et al., 2007; Twohy et al., 2009; Bar-Or et al., 2011a). Here we explore the optical behavior of different types of aerosols in vicinity of clouds using the Spherical Harmonic Discrete Ordinate Method model for atmospheric radiative transfer (SHDOM, Evans, 1998). To do so, we focus on the change in total extinction (in units of km^{-1}), the single scattering albedo (ω), and the asymmetry parameter (g) as a function of distance from the nearest cloud (d_c) at wavelengths of 532 nm and 355 nm.

In each simulation the hygroscopicity parameter κ (Petters and Kreidenweis, 2007), the real part of the dry aerosol complex refractive index, the dry effective diameter ($D_{eff-dry}$), assuming a single-mode log-normal distribution with a $\ln(\sigma) = 0.7$, and the mass of the aerosol layer, set at 5 µg m^{-3}, are kept constant while varying the imaginary

ACPD
12, 1019–1052, 2012

part of the dry aerosol RI. Moreover, two different RH fields are used in the model: one typical for the marine boundary layer (MBL), where the background RH reaches ~88 %, and the other describing continental cumulus cloud field (CCF) where the background RH reaches 60 %. Both RH fields are extracted from large-eddy-simulation model results (UCLA-LES, Xue and Feingold, JAS, 2006, and RAMS, Cotton et al., 2003), and supported by in-situ measurements (Twohy et al., 2009; Wang and Geerts, 2010). Only distances of up to 0.5 km from the nearest cloud are shown, since relative humidity changes beyond this point found negligible (Bar-Or et al., 2011b). The κ values used are $\kappa = 0.6$, typical of ammonium sulfate (Petters and Kreidenweis, 2007) and $\kappa = 0.15$, typical of organic aerosols (Petters et al., 2009). The real part of the RI and the dry effective diameters used are $n = 1.504$ and $n = 1.626$, and $D_{\mathrm{eff-dry}} = 0.1\,\mu\mathrm{m}$ and $D_{\mathrm{eff-dry}} = 0.2\,\mu\mathrm{m}$. The imaginary component of the RI for the dry aerosols was varied from 0.0 to 0.4 in 0.05 steps. The results for the extinction as a function of distance from the nearest cloud (d_c) are shown in Fig. 6, for SSA (ω) vs. d_c in Fig. 7, and for the asymmetry parameter vs. d_c in Fig. 8. Both figures show 4 pairs of graphs, where within each pair all variables are the same except the RH field; left side MBL and right side CCF. The top graphs (a-MBL, a-CCF, b-MBL, b-CCF) show the simulations for a $D_{\mathrm{eff-dry}} = 0.1\,\mu\mathrm{m}$, where the lower graphs (c-MBL, c-CCF, d-MBL, d-CCF) for a $D_{\mathrm{eff-dry}} = 0.2\,\mu\mathrm{m}$. The differences within the top and lower graphs are the κ and n values. The left graphs have a $\kappa = 0.6$ and $n = 1.504$, where the right graphs have a $\kappa = 0.15$ and $n = 1.626$.

In Fig. 6 we observe that the extinction is practically independent from the imaginary component of the complex refractive index, and that for a $D_{\mathrm{eff-dry}} = 0.2\,\mu\mathrm{m}$ there is even no spectral dependence. Furthermore, the greatest differences in extinction occur in the first 50 m near the cloud edge, with a steep exponential increase, further away the extinction remains practically constant for all of the CCF cases, and it decreases slightly for the MBL cases; a maximum of $0.07\,\mathrm{km}^{-1}$ for the a-MBL case. For the MBL case study the differences in extinction are dominated more by the size of the effective dry diameter than by differences in κ or n, we can see that between a-MBL and b-MBL

ACPD
12, 1019–1052, 2012

the shape and value of the extinction are basically the same (as well as between c-MBL and d-MBL). This suggests that the dry size distribution of the aerosols present in the twilight zone is the dominant factor in the total extinction. For the CCF cases we see a greater difference in the extinction between the constant $D_{\mathrm{eff-dry}}$ with different κ and n, where below an RH of 80 % the real part of the RI dominates. For example, there is around a 0.01 km^{-1} difference in extinction between a-CCF and b-CCF, which means that for an aerosol layer of 5 km there is an optical depth difference of 0.05 which is small but not negligible.

On the contrary to the extinction as a function of d_c, we observe clear difference in the single scattering albedo (Fig. 7) and asymmetry parameter (Fig. 8) vs. d_c, for different degrees of absorption of the present aerosols. In Fig. 7 we see that in the first 50 m from the cloud edge there are significant differences between the highly absorbing ($k = 0.4$) and lightly absorbing ($k = 0.05$) aerosol. Within this distance, the single scattering albedo may decrease down to $\omega = 0.45$ for an imaginary component of $k = 0.4$, and down to $\omega = 0.75$ for $k = 0.05$ at a wavelength of 355 nm (see d-CCF) and 532 nm (see b-CCF). We also see that the value of ω for a specific imaginary component at different d_c's varies for each of the 8 cases presented. For the MBL cases, there is a constant decrease in ω as the d_c increases, whereas for the CCF cases after the first 100 m the single scattering albedo remains constant. Another distinct feature in the behavior of ω is that it is always lower at 355 nm than at 532 nm for the same k value, with the exception of the $k = 0.4$ value of the b-CCF case. For the $D_{\mathrm{eff-dry}} = 0.2$ µm cases the differences between the wavelengths is greater than at $D_{\mathrm{eff-dry}} = 0.1$ µm.

From the asymmetry parameter (Fig. 8) we see that the light is predominantly scattered to the forward direction for both wavelengths, with generally being larger for 355 nm than for 532 nm for the same k value (see c-MBL for the few exceptions). Furthermore, the asymmetry parameter goes from a minimum value for purely scattering aerosols, with values as low as $g = 0.66$ at 532 nm (b-CCF), to a maximum value for the highly absorbing aerosols; i.e., as the imaginary component is increased the scatter light is directed more in the forward direction. We also observe that there is

ACPD
12, 1019–1052, 2012

not a clear pattern on how the asymmetry parameter changes with d_c. For example, at 355 nm g tends to sharply increase for $d_c < 50$ m, with the exception of b-CCF, whereas for 532 nm it can remain fairly constant (see c-CCF and d-MBL), decrease rapidly (see b-MBL and b-CCF), or increase (c-MBL and a-MBL). Only after 0.2 km away from the cloud is that g remains constant for all cases.

6 Discussion

From the laboratory measurements we see that $f\mathrm{RH}_{\mathrm{ext}}$ at 80 % and 90 % RH could be modeled using Mie theory, the hygroscopic growth factor, and the dry refractive indices of the water soluble absorbing aerosols; there is closure between measured and modeled $f\mathrm{RH}_{\mathrm{ext}}$ values as a function of size. We also observe that the $f\mathrm{RH}_{\mathrm{ext}}$ dependence on size changes from having an exponential dependence for purely scattering substances to demonstrating practically no dependence for absorbing substances with an imaginary part greater than zero.

Moreover, the small discrepancies between the retrieved complex RI from direct measurements at 355 nm and 532 nm and the complex RI calculated from the volume weighted mixing rule suggest the volume weighted mixing rule is a good approximation for water soluble aerosols at high RH conditions; especially for substances with GF > 1.15. The difference between the derived and calculated real parts of the complex RIs were less than 5.3 % for all substances, wavelengths, and RHs. The obtained imaginary parts for the retrieved and calculated RIs were in good agreement with each other, and well within the measurement errors of retrieval from pulsed CRD spectroscopy measurements. On the other hand, the homogenous mixture assumption for particles with small GF (less than 1.15) needs to be taken with caution for size parameter greater than 2.5. By modeling a core-shell structure versus a homogenously mixed particle we find difference between the two models that can exceed 10 %. For size parameters less than 2.5 at 80 % RH there is less than a 5 % difference between the extinction efficiencies calculated with the two models. This difference is within

ACPD
12, 1019–1052, 2012

measurement errors; hence, there is no significant optical difference between the two assumptions of the internal structure of the particles. For 90 % RH the differences below a size parameter of 2.5 increase up to 7 %.

In our "twilight zone" simulations we assumed one type of aerosols present in the edge of the cloud, which implies that all present aerosols are activated with the increase in RH, and we assumed that the concentration of the aerosols is constant throughout d_c. Twohy et al. (2009) showed that the particle concentration near clouds does not change significantly, except within 100 m of the cloud edge. This increase near the cloud edge will make the slope in the extinction simulations steeper, but will not change the behavior of the curves with different k values. Regarding the assumption of one present type of aerosols, during INDOEX (Indian Ocean Experiment) Rajeev et al. (2000) found that 80 % of the aerosol was composed of soot and the remaining 20 % were water soluble substances (sulfate, ammonia, nitrate, and organics). Twohy et al. (2009) used this data to analyze aerosol scattering near clouds, and found that the increase in the scattering cross section near clouds is independent of the aerosol composition when considering an externally mixed aerosol; they found that more than 90 % of the scattering could be contributed by the water soluble components at RH > 70 %. In the study by Twohy et al. (2009) it was implied that soot is hydrophobic, however, recently Spracklen et al. (2011) analyzed the role of carbonaceous combustion aerosols as cloud condensation nuclei (CCN), and found that carbonaceous combustion aerosols can contribute 52–64 % to simulated global mean surface level CCN concentrations. This result suggests that even though fresh soot is hydrophobic, atmospheric processing (aging) makes it a good CCN. The results found by Twohy et al. (2009) and Spracklen et al. (2011) allowed the assumptions taken in our simulations to be more "realistic", though the results we see are to be taken as hypothesized concepts to help understand the limits of the conditions that might be present.

The rapid decay in the extinction signal in the first 100 m near the cloud edge brings the questions of how significant are the results seen for the extinction, single scattering albedo, and asymmetry parameter. In terms of remote sensing, these properties are

ACPD
12, 1019–1052, 2012

probably not very significant, since the scales are too small. In terms of radiative forcing? The forcing depends heavily on the fractal dimension D of the cloud field. When the morphology is simple ($D \sim = 1$) the cloud edges occupy limited portion of the field and therefore changes in the first 0.5 km from the cloud edge will probably not contribute significantly. However, in cases of higher fractal dimension such as trade cumulus filed, the area in the vicinity of cloud edges can occupy most of the cloud free area and the results observed in the simulations can have significant implications. We can observe from the extinction vs. d_c graphs that regardless of the absorption of the aerosol population the total extinction barely changes. On the contrary, the single scattering albedo, as expected, and the asymmetry parameter show sharp differences with respect to the value of the imaginary component of the RI. We can see that for purely scattering or lightly absorbing aerosols, the light is redistributed more equally (g is closer to 0.5), whereas for the highly absorbing aerosols the scattered light is redirected more to the forward (g closer to one). This tells us that as the imaginary component of the RI increases, the reflectivity of the aerosol layer decreases, reducing the cooling effect of aerosols in the layer present and at the surface. Moreover, the scattering contribution from the cloud edge, cloud 3D radiative effects (Marshak et al., 2006; Varnai and Marshak, 2009), are probably reduced with more absorbing aerosols.

Acknowledgements. Funding was provided by the Israel Science Foundation (Grant #196/08) and by FP7-ENV-2010-265148-PEGASOS. This research was also funded by the Max Planck Institute internal funding. Y. R. acknowledges support by the Helen and Martin Kimmel Award for Innovative Investigation.

The service charges for this open access publication have been covered by the Max Planck Society.

References

Abo Riziq, A., Erlick, C., Dinar, E., and Rudich, Y.: Optical properties of absorbing and non-absorbing aerosols retrieved by cavity ring down (CRD) spectroscopy, Atmos. Chem. Phys.,

7, 1523–1536, doi:10.5194/acp-7-1523-2007, 2007.
Bar-Or, R. Z., Altaratz, O., and Koren, I.: Global analysis of cloud field coverage and radiative properties, using morphological methods and MODIS observations, Atmos. Chem. Phys., 11, 191–200, doi:10.5194/acp-11-191-2011, 2011a.
Bar-Or, R. Z., Koren, I., Altaratz, O., and Fredj, E.: Radiative properties of humidified aerosol in cloudy enviroenment, Atmos. Chem. Phys. Discuss., in preparation, 2011b.
Baynard, T., Garland, R. M., Ravishankara, A. R., Tolbert, M. A., and Lovejoy, E. R.: Key factors influencing the relative humidity dependence of aerosol light scattering, Geophys. Res. Lett., 33, L06813, doi:10.1029/2005gl024898, 2006.
Bohren C. F. and Huffman D. R.: Absorption and scattering of light by small particles, Wiley, New York, USA, 1983.
Brooks, S. D., DeMott, P. J., and Kreidenweis, S. M.: Water uptake by particles containing humic materials and mixtures of humic materials with ammonium sulfate, Atmos. Environ., 38, 1859–1868, 2004.
Cotton, W. R., Pielke, R. A., Walko, R. L., Liston, G. E., Tremback, C. J., Jiang, H., McAnelly, R. L., Harrington, J. Y., Nicholls, M. E., Carrio, G. G., and McFadden, J. P.: Rams 2001: Current status and future directions, Meteorol. Atmos. Phys., 82, 5–29, doi:10.1007/s00703-001-0584-9, 2003.
Daimon, M. and Masumura, A.: Measurement of the refractive index of distilled water from the near-infrared region to the ultraviolet region, Appl. Opt., 46, 3811–3820, 2007.
Dinar, E., I. Taraniuk, E. R. Graber, T. Anttila, T. F. Mentel, and Y. Rudich: Hygroscopic growth of atmospheric and model humic-like substances, J. Geophys. Res., 112, D05211, doi:10.1029/2006JD007442, 2007.
Dinar, E., Riziq, A. A., Spindler, C., Erlick, C., Kiss, G., and Rudich, Y.: The complex refractive index of atmospheric and model humic-like substances (hulis) retrieved by a cavity ring down aerosol spectrometer (crd-as), Faraday Discuss., 137, 279–295, doi:10.1039/b703111d, 2008.
Dusek, U., Reischl, G. P., and Hitzenberger, R.: CCN activation of pure and coated carbon black particles, Environ. Sci. Technol, 40, 1223–1230, 2006.
Erlick, C.: Effective refractive indices of water and sulfate drops containing absorbing inclusions, J. Atmos. Sci., 63, 754–763, 2006.
Evans, K. F.: The spherical harmonics discrete ordinate method for three-dimensional atmospheric radiative tranfer, J. Atmos. Sci., 55, 429–446, doi:10.1175/1520-

ACPD
12, 1019–1052, 2012

0469(1998)055<0429:TSHDOM>2.0.CO;2, 1998.
Garland, R. M., Ravishankara, A. R., Lovejoy, E. R., Tolbert, M. A., and Baynard, T.: Parameterization for the relative humidity dependence of light extinction: Organic-ammonium sulfate aerosol, J. Geophys. Res., 112, D19303, doi:10.1029/2006JD008179., 2007.
Gysel, M., Weingartner, E., and Baltensperger, U.: Hygroscopicity of aerosol particles at low temperatures. 2. Theoretical and experimental hygroscopic properties of laboratory generated aerosols, Environ. Sci. Technol., 36, 63–68, doi:10.1021/es010055g, 2002.
Hansen, J., Sato, M., Ruedy, R., Nazarenko, L., Lacis, A., Schmidt, G. A., Russell, G., Aleinov, I., Bauer, M., Bauer, S., Bell, N., Cairns, B., Canuto, V., Chandler, M., Cheng, Y., Del Genio, A., Faluvegi, G., Fleming, E., Friend, A., Hall, T., Jackman, C., Kelley, M., Kiang, N., Koch, D., Lean, J., Lerner, J., Lo, K., Menon, S., Miller, R., Minnis, P., Novakov, T., Oinas, V., Perlwitz, J., Perlwitz, J., Rind, D., Romanou, A., Shindell, D., Stone, P., Sun, S., Tausnev, N., Thresher, D., Wielicki, B., Wong, T., Yao, M., and Zhang, S.: Efficacy of climate forcings, J. Geophys. Res.-Atmos., 110, D18104, doi:10.1029/2005JD005776, 2005.
Hasenkopf, C. A., Freedman, M. A., Beaver, M. R., Toon, O. B., and Tolbert, M. A.: Potential climatic impact of organic haze on early earth, Astrobiology, 11, 135–149, doi:10.1089/ast.2010.0541, 2011.
Haywood, J. M., Roberts, D. L., Slingo, A., Edwards, J. M., and Shine, K. P.: General circulation model calculations of the direct radiative forcing by anthropogenic sulfate and fossil-fuel soot aerosol, J. Climate, 10, 1562–1577, doi:10.1175/1520-0442(1997)010¡1562:GCMCOT¿2.0.CO;2, 1997.
Hoppel, W.: Determination of the aerosol size distribution from the mobility distribution of the charged fraction of aerosols, J. Aerosol Sci., 9, 41–54, 1978.
Jacobson, M. Z.: Global direct radiative forcing due to multicomponent anthropogenic and natural aerosols, J. Geophys. Res.-Atmos., 106, 1551–1568, 2001.
Jacobson, M. Z.: Effects of externally-through-internally-mixed soot inclusions within clouds and precipitation on global climate, J. Phys. Chem. A, 110, 6860–6873, doi:10.1021/jp056391r, 2006.
Kanakidou, M., Seinfeld, J. H., Pandis, S. N., Barnes, I., Dentener, F. J., Facchini, M. C., Van Dingenen, R., Ervens, B., Nenes, A., Nielsen, C. J., Swietlicki, E., Putaud, J. P., Balkanski, Y., Fuzzi, S., Horth, J., Moortgat, G. K., Winterhalter, R., Myhre, C. E. L., Tsigaridis, K., Vignati, E., Stephanou, E. G., and Wilson, J.: Organic aerosol and global climate modelling: a review, Atmos. Chem. Phys., 5, 1053–1123, doi:10.5194/acp-5-1053-2005, 2005.

ACPD
12, 1019–1052, 2012

Kaufman, Y. J., Koren, I., Remer, L. A., Rosenfeld, D., and Rudich, Y.: The effect of smoke, dust, and pollution aerosol on shallow cloud development over the atlantic ocean, P. Natl. Acad. Sci. USA, 102, 11207–11212, 2005.
Koren, I., Kaufman, Y. J., Remer, L. A., and Martins, J. V.: Measurement of the effect of amazon smoke on inhibition of cloud formation, Science, 303, 1342–1345, 2004.
Koren, I., Remer, L. A., Kaufman, Y. J., Rudich, Y., and Martins, J. V.: On the twilight zone between clouds and aerosols, Geophys. Res. Lett., 34, L08805, doi:10.1029/2007gl029253, 2007.
Lack, D. A., Lovejoy, E. R., Baynard, T., Pettersson, A., and Ravishankara, A. R.: Aerosol absorption measurement using photoacoustic spectroscopy: Sensitivity, calibration, and uncertainty developments, Aerosol Sci. Tech., 40, 697–708, 2006.
Lang-Yona, M., Rudich, Y., Segre, E., Dinar, E., and Abo-Riziq, A.: Complex refractive indices of aerosols retrieved by continuous wave-cavity ring down aerosol spectrometer, Anal. Chem., 81, 1762–1769, doi:10.1021/ac8017789, 2009.
Lang-Yona, N., Rudich, Y., Mentel, Th. F., Bohne, A., Buchholz, A., Kiendler-Scharr, A., Kleist, E., Spindler, C., Tillmann, R., and Wildt, J.: The chemical and microphysical properties of secondary organic aerosols from Holm Oak emissions, Atmos. Chem. Phys., 10, 7253–7265, doi:10.5194/acp-10-7253-2010, 2010.
Liu, L., Wang, H., Yu, B., Xu, Y., and Shem, J.: Improved algorithm of light scattering by a coated sphere, China Part., 5, 230–236, 2007a.
Liu, X., Penner, J. E., Das, B., Bergmann, D., Rodriguez, J. M., Strahan, S., Wang, M., and Feng, Y.: Uncertainties in global aerosol simulations: Assessment using three meteorological data sets, J. Geophys. Res., 112, D11212, doi:10.1029/2006jd008216, 2007b.
Marshak, A., Platnick, S., Varnai, T., Wen, G. Y., and Cahalan, R. F.: Impact of three-dimensional radiative effects on satellite retrievals of cloud droplet sizes, J. Geophys. Res.-Atmos., 111, D09207, doi:10.1029/2005jd006686, 2006.
Menon, S., Hansen, J., Nazarenko, L., and Luo, Y. F.: Climate effects of black carbon aerosols in china and india, Science, 297, 2250–2253, 2002.
Petters, M. D. and Kreidenweis, S. M.: A single parameter representation of hygroscopic growth and cloud condensation nucleus activity, Atmos. Chem. Phys., 7, 1961–1971, doi:10.5194/acp-7-1961-2007, 2007.
Petters, M. D., Carrico, C. M., Kreidenweis, S. M., Prenni, A. J., DeMott, P. J., Collett, J. L., and Moosmüller, H.: Cloud condensation nucleation activity of biomass burning aerosol, J.

ACPD
12, 1019–1052, 2012

Geophys. Res.-Atmos., 114, D22205, doi:10.1029/2009jd012353, 2009.
Pettersson, A., Lovejoy, E. R., Brock, C. A., Brown, S. S., and Ravishankara, A. R.: Measurement of aerosol optical extinction at 532 nm with pulsed cavity ring down spectroscopy, J. Aerosol Sci., 35, 995–1011, do:10.1016/j.jaerosci.2004.02.008, 2004.
Rajeev, K., Ramanathan, V., and Meywerk, J.: Regional aerosol distribution and its long-range transport over the Indian Ocean, J. Geophys. Res., 105, 2029–2043, 2000.
Sappey, A. D., Hill, E. S., Settersten, T., and Linne, M. A.: Fixed-frequency cavity ringdown diagnostic for atmospheric particulate matter, Opt. Lett., 23, 954–956, 1998.
Sjogren, S., Gysel, M., Weingartner, E., Baltensperger, U., Cubison, M. J., Coe, H., Zardini, A. A., Marcolli, C., Krieger, U. K., and Peter, T.: Hygroscopic growth and water uptake kinetics of two-phase aerosol particles consisting of ammonium sulfate, adipic and humic acid mixtures, J. Aerosol Sci., 38, 157–171, doi:10.1016/j.jaerosci.2006.11.005, 2007.
Smith, J. D. and Atkinson, D. B.: A portable pulsed cavity ringdown transmissometer for measurement of the optical extinction of the atmospheric aerosol, Analyst, 126, 1216–1220, 2001.
Spracklen, D. V., Carslaw, K. S., Pöschl, U., Rap, A., and Forster, P. M.: Global cloud condensation nuclei influenced by carbonaceous combustion aerosol, Atmos. Chem. Phys., 11, 9067–9087, doi:10.5194/acp-11-9067-2011, 2011.
Stokes, R. H., Robinson, R. A. : Interactions in aqueous nonelectrolyte solutions. I. Solute-solvent equilibria, J. Phys. Chem., 70, 2126–2130, 1966.
Twohy, C. H., Coakley, J. A., and Tahnk, W. R.: Effect of changes in relative humidity on aerosol scattering near clouds, J. Geophys. Res.-Atmos., 114, D05205, doi:10.1029/2008jd010991, 2009.
Varnai, T. and Marshak, A.: Modis observations of enhanced clear sky reflectance near clouds, Geophys. Res. Lett., 36, L06807, doi:10.1029/2008gl037089, 2009.
Wang, Y. and Geerts, B.: Humidity variations across the edge of trade wind cumuli: Observations and dynamical implications, Atmos. Res., 97, 144–156, doi:10.1016/j.atmosres.2010.03.017, 2010.
Wild, M.: Solar radiation budgets in atmospheric model intercomparisons from a surface perspective, Geophys. Res. Lett., 32, L07704, doi:10.1029/2005gl022421, 2005.
Xue, H. W. and Feingold, G: Large-eddy simulations of trade wind cumuli: Investigation of aerosol indirect effects, J. Atmos. Sci., 63, 1605–1622, doi:10.1175/JAS3706.1, 2006.
Yu, H., Kaufman, Y. J., Chin, M., Feingold, G., Remer, L. A., Anderson, T. L., Balkanski, Y.,

ACPD
12, 1019–1052, 2012

Bellouin, N., Boucher, O., Christopher, S., DeCola, P., Kahn, R., Koch, D., Loeb, N., Reddy, M. S., Schulz, M., Takemura, T., and Zhou, M.: A review of measurement-based assessments of the aerosol direct radiative effect and forcing, Atmos. Chem. Phys., 6, 613–666, doi:10.5194/acp-6-613-2006, 2006.

ACPD
12, 1019–1052, 2012

Table 1. Measured $f\mathrm{RH}_{\mathrm{ext}}$ (80 % RH, Dry) as a function of size (solid circles) for pure ammonium sulfate. The dashed line shows the exponential fit from the measurements performed by Garland et al. (2007) for ammonium sulfate at the same RH. The shaded area is the calculated $f\mathrm{RH}_{\mathrm{ext}}$(80 % RH, Dry) range, based on the growth factors measured with the SMPS.

			532 nm		355 nm	
	Dry refractive index		m=1.504(±0.015) + *i*0.0(±0.028)		m=1.507(±0.024) + *i*0.005(±0.025)	
			80% RH	**90% RH**	**80% RH**	**90% RH**
Ammonium sulfate	Growth Factor	This study	1.44(±0.02)	1.77(±0.25)	1.44(±0.02)	1.77(±0.25)
		Literature	1.46 (±0.01)[a,b,c]	1.69(±0.01)[a,b]	1.46 (±0.01)[a,b,c]	1.69(±0.01)[a,b]
		% Difference	1.4	4.6	1.4	4.6
	Ref. Index	Volume Weighted	m=1.39(±0.02) + *i*0.0	m=1.370(±0.02) + *i*0.0	1.40(±0.02) + i0.00(±0.03)	1.39(±0.02) + i0.00(±0.03)
		Retrieved	m=1.437(±0.03) + *i*0.02(±0.04)	m=1.328(±0.01) + *i*0.0(±0.03)	1.42(±0.03) + i0.0(±0.04)	1.41(±0.06) + i0.0 (±0.04)
		% Diff (n)+i(k)	3 + *i*200	3.1 + *i*0	1.5 + i0	2.6 + i0
IHSS Pahokee peat	Dry refractive index		m=1.558(±0.005) + *i*0.033(±0.007)		m=1.541(±0.034) + i0.18(±0.066)	
	Growth Factor	This study	1.09(±0.01)	1.17(±0.02)	1.09(±0.01)	1.37(±0.02)[f]
		Literature	1.07(±0.01)[d]	1.12(±0.01)[d]	1.07(±0.01)[d]	1.23(±0.01)[d]
		% Diff	1.85	4.4	1.85	10.8
	Ref. Index	Volume Weighted	m=1.514(±0.004) + *i*0.026(±0.007)	m=1.503(±0.009) + *i*0.025(±0.007)	1.497(±0.034) + i0.139(±0.066)	1.424(±0.034) + i0.07(±0.066)
		Retrieved	m=1.495(±0.006) + *i*0.053(±0.009)	m=1.517(±0.008) + *i*0.025(±0.014)	1.578(±0.047) + i0.171(±0.072)	1.415(±0.045) + i0.064(±0.053)
		% Diff (n)+i(k)	1.3 + *i*68	0.9 + *i*0	5.3 + i20	0.6 + i8.9

ACPD
12, 1019–1052, 2012

Table 1. Continued.

AS :Nig[g]	Dry refractive index		m=1.595(±0.031) + *i*0.154(±0.021)		m=1.431(±0.034) + i0.178(±0.066)	
	Growth Factor	This study	1.28(±0.02)	1.45(±0.02)	1.28(±0.02)	1.45(±0.02)
		Literature	1.29(±0.02)[e]	1.45(±0.1)[e]	1.29(±0.02)[e]	1.45(±0.1)[e]
		% Diff	0.8	0	0.8	0
	Ref. Index	Volume Weighted	m=1.431(±0.031) + *i*0.084(±0.021)	m=1.396(±0.031) + *i*0.046(±0.021)	1.388(±0.034) + i0.084(±0.066)	1.378(±0.034) + i0.058(±0.066)
		Retrieved	m=1.40(±0.01) + *i*0.086(±0.013)	m=1.329(±0.008) + *i*0.04(±0.017)	1.402(±0.037) + i0.079(±0.058)	1.377(±0.05) + i0.087(±0.064)
		% Diff (n)+i(k)	2.2 + *i*2.3	4.9 + *i*14	1.0 + i6	0.01 + i40
Nigrosine	Dry refractive index		m=1.626(±0.021) + *i*0.243(±0.023)		m=1.568(±0.056) + i0.305(±0.171)	
	Growth Factor	This study	1.12(±0.02)	1.24(±0.1)	1.12(±0.02)	1.24(±0.1)
		Literature	1.15[h]	1.34[h]	1.15[h]	1.34[h]
		% Diff	2.6	7.8	2.6	7.8
	Ref. Index	Volume Weighted	m=1.544(±0.021) + *i*0.174(±0.023)	m=1.493(±0.021) + *i*0.132(±0.023)	1.508(±0.056) + i0.217(±0.171)	1.465(±0.056) + i0.160(±0.171)
		Retrieved	m=1.464(±0.004) + *i*0.216(±0.014)	m=1.504(±0.012) + *i*0.168(±0.024)	1.542(±0.066) + i0.249(±0.14)	1.477(±0.058) + i0.145(±0.087)
		% Diff (n)+i(k)	5.3 + *i*21.5	0.7 + *i*24	2.2 + i14	0.8 + i9.8

[a] Gysel et al., 2002; [b] Dinar et al., 2008; [c] Sjogren et al., 2007; [d] Brooks et al., 2004 [f] Measurement performed at 95 % RH; [e] Derived using the ZSR relation; [g] 1:1 molar ratio. [h] Taken from: https://sciencepolicy.colorado.edu/events/rendezvous/2007/posters/II21K.pdf.

ACPD
12, 1019–1052, 2012

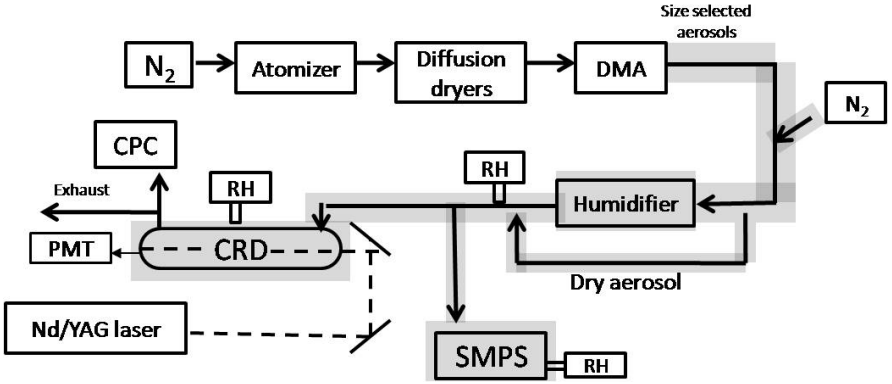

Fig. 1. Schematic of the laboratory setup. The bold arrows show the aerosol flow and the dotted lines represent the laser's light paths. The temperature and relative humidity meters are marked as "RH". Abbreviations: CPC, condensation particle counter; PMT, photomultiplier; DMA, differential mobility analyzer.

ACPD
12, 1019–1052, 2012

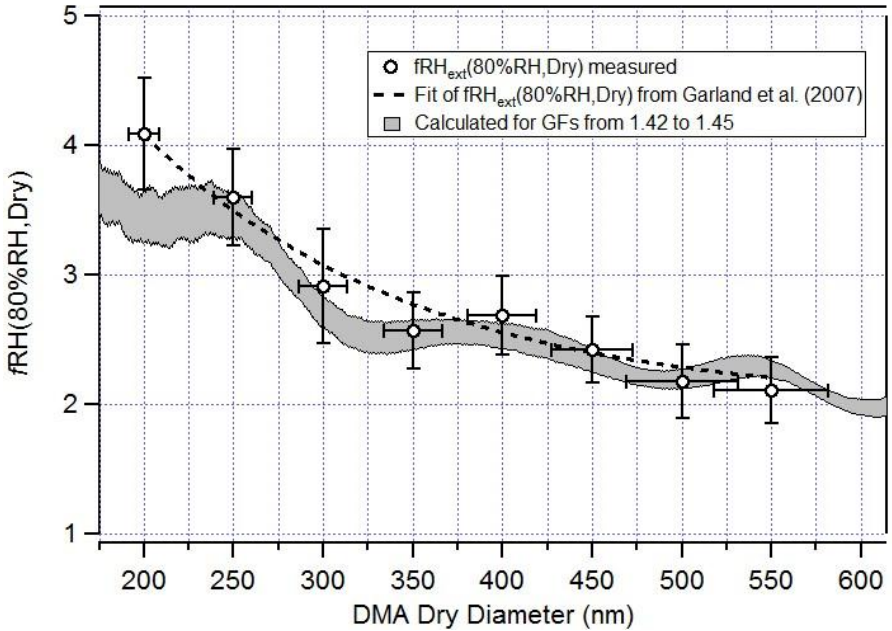

Fig. 2. Size dependence of $f\mathrm{RH}_{ext}$(80 %RH, Dry) **(a)** and $f\mathrm{RH}_{ext}$(90 %RH, Dry) **(b)** for pure ammonium sulfate (top panel; circles), IHSS Pahokee peat (inverted triangles). the mixture of ammonium sulfate and nigrosine at 1:1 molar ratio (squares), and pure nigrosine (triangles) at 532 nm(full green markers) and 355 nm (open blue markers). The shaded areas represent the theoretical size dependence calculated from the measured growth factors from the SMPS. The data for the growth factors are indicated in the legend.

ACPD
12, 1019–1052, 2012

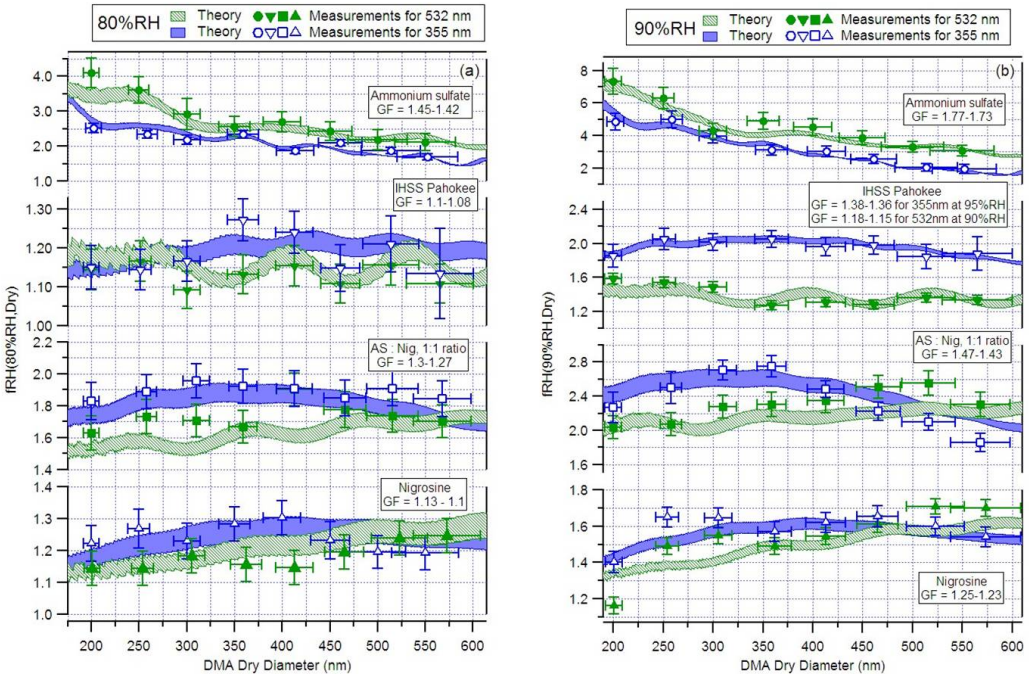

Fig. 3. Extinction efficiency vs. size at 80 % RH for **(a)** Pahokee peat and **(b)** Nigrosine aerosol. The open circles represent the measured $Q_{ext,80\,\%\ RH}$ using the measured hygroscopic growth. The dotted line is the Q_{ext} curve for the retrieved RI from the $Q_{ext,\%RH}$ measurements. The solid line shows the expected Q_{ext} curve from the calculated RI assuming homogeneous mixing and using a volume weighted mixing rule to calculate the complex refractive index. The solid squares represent the Q_{ext} values if a core-shell structure is assumed.

ACPD
12, 1019–1052, 2012

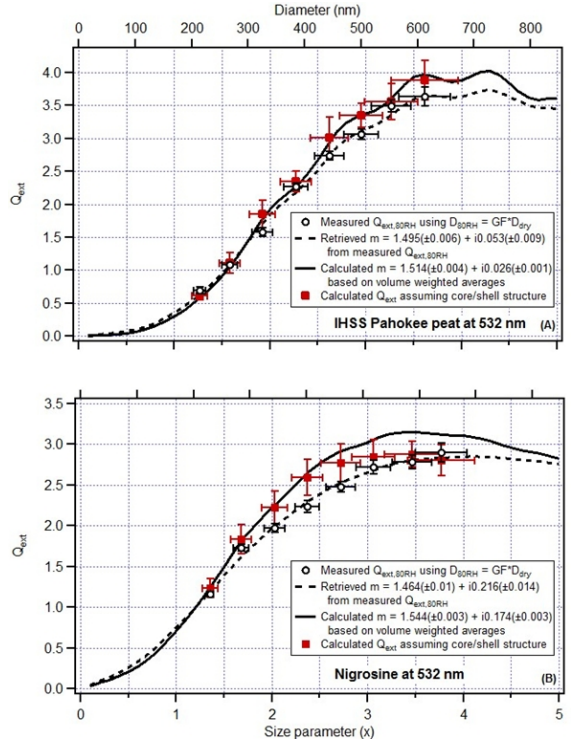

Fig. 4. Extinction as a function of distance from the nearest cloud (d_c), for four different scenarios: **(a)** the hygroscopicity parameter (κ) set at 0.6, the real part of the refractive index (n) set at 1.504, and the dry effective diameter ($D_{\text{eff-dry}}$) set at 0.1 µm; **(b)** κ=0.15, n=1.626, and $D_{\text{eff-dry}}$= 0.1 µm; **(c)** κ=0.6, n=1.504, and $D_{\text{eff-dry}}$= 0.2 µm; **(d)** κ = 0.15, n = 1.626, and $D_{\text{eff-dry}}$= 0.2 µm. For each scenario two different relative humidity fields were used: one typical for the marine boundary layer (MBL), and the other describing a continental Cumulus cloud field (CCF). Two wavelengths: 355 nm (solid lines) and 532 nm (dashed lines), are shown. The imaginary component (color scale) was varied in each case from 0 to 0.4.

ACPD
12, 1019–1052, 2012

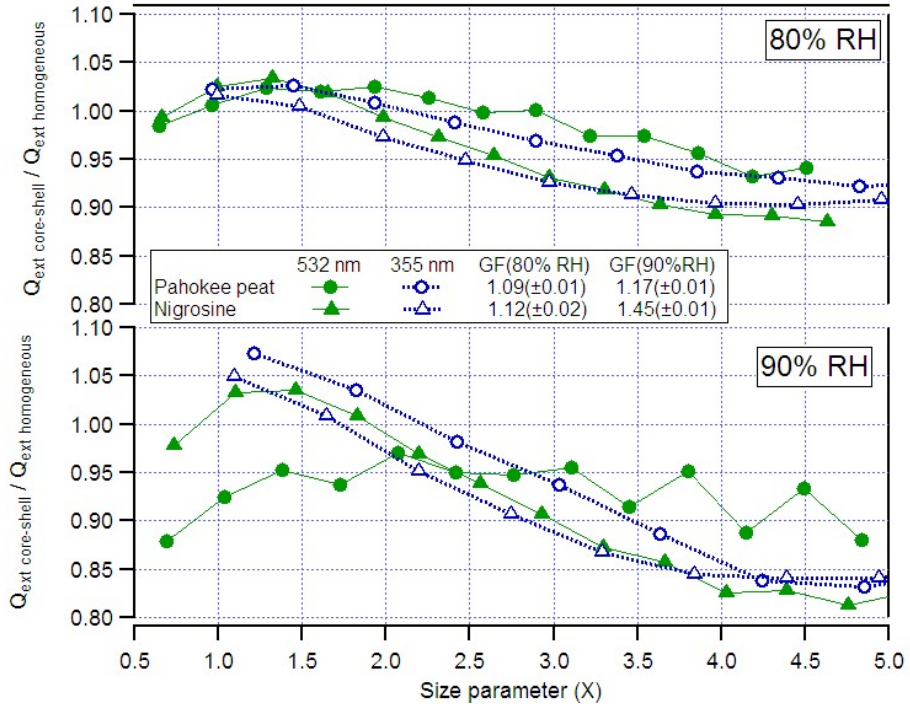

Fig. 5. Single scattering albedo (ω) as a function of distance from the nearest cloud (d_c) for the same scenarios as in Fig. 7. See Fig. 7 caption for full description.

ACPD
12, 1019–1052, 2012

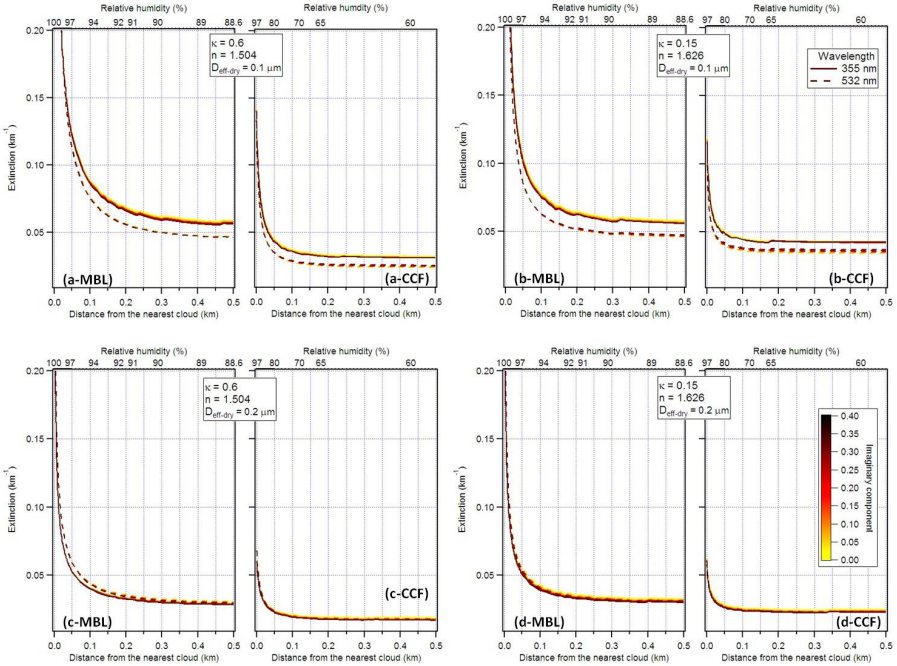

Fig. 6. Asymmetry parameter (g) as a function of distance from the nearest cloud (d_c) for the same scenarios as in Figs. 7 and 8. See Fig. 7 caption for full description.

ACPD
12, 1019–1052, 2012

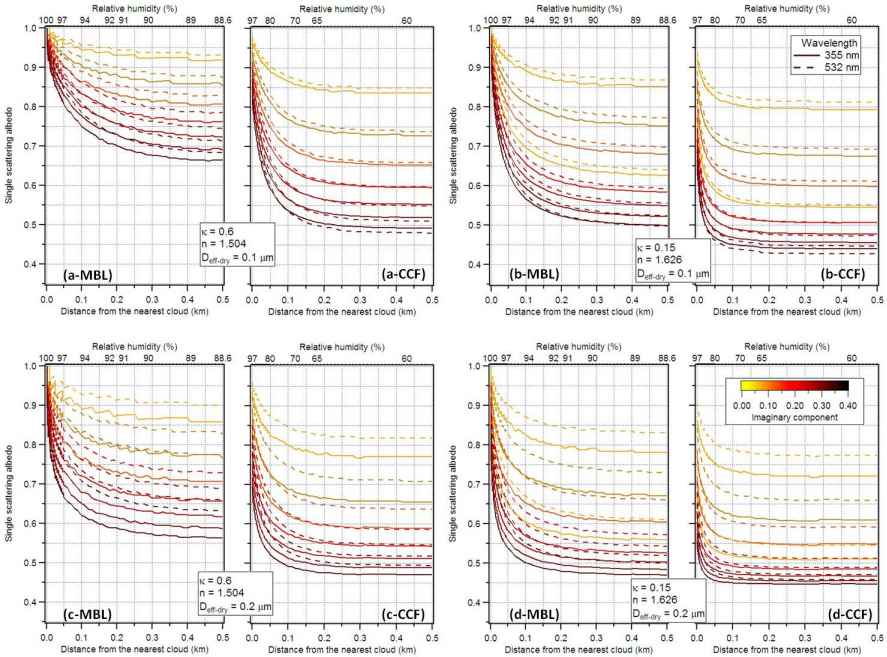

Fig. 7. Single scattering albedo (ω) as a function of distance from the nearest cloud (d_c) for the same scenarios as in Fig. 7. See Fig. 7 caption for full description.

ACPD
12, 1019–1052, 2012

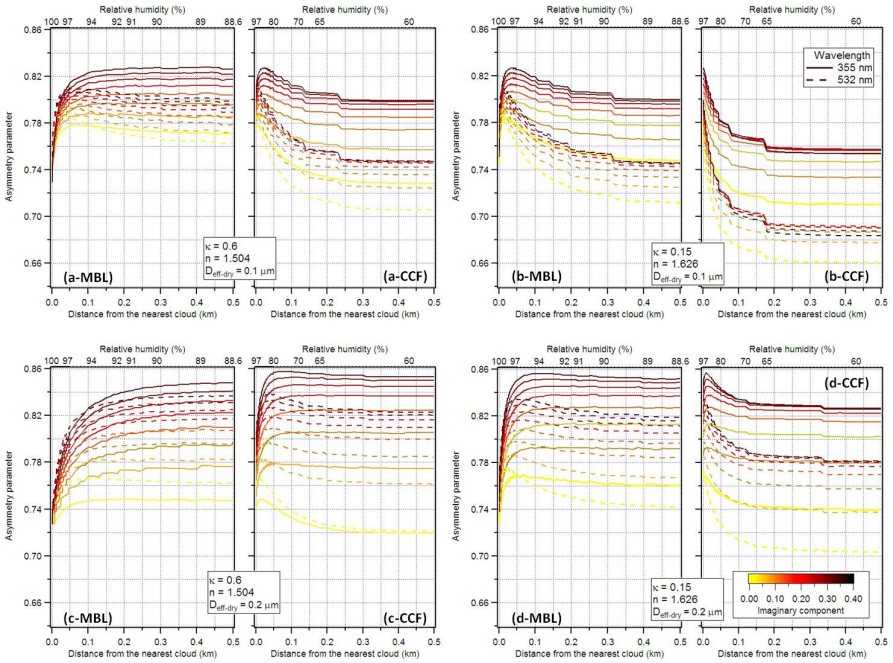

Fig. 8. Asymmetry parameter (g) as a function of distance from the nearest cloud (d_c) for the same scenarios as in Figs. 7 and 8. See Fig. 7 caption for full description.

ACPD
12, 1019–1052, 2012